Study of the $\eta_c(1\,^1S_0)$ state of charmonium formed in $\bar{p}p$ annihilations and a search for the $\eta_c'(2\,^1S_0)$

T.A. Armstrong,[6] D. Bettoni,[2] V. Bharadwaj,[1] C. Biino,[7] G. Blanford,[4] G. Borreani,[7] D. Broemmelsiek,[4] A. Buzzo,[3] R. Calabrese,[2] A. Ceccucci,[7] R. Cester,[7] M. Church,[1] P. Dalpiaz,[2] P.F. Dalpiaz,[2] D. Dimitroyannis,[5] M. Fabbri,[2] J. Fast,[4] A. Gianoli,[2] C.M. Ginsburg,[5] K. Gollwitzer,[4] G. Govi,[7] A. Hahn,[1] M. Hasan,[6] S. Hsueh,[1] R. Lewis,[6] E. Luppi,[2] M. Macrí,[3] A.M. Majewska,[6] M. Mandelkern,[4] F. Marchetto,[7] M. Marinelli,[3] J. Marques,[4] W. Marsh,[1] M. Martini,[2] M. Masuzawa,[5] E. Menichetti,[7] A. Migliori,[7] R. Mussa,[7] S. Palestini,[7] M. Pallavicini,[3] S. Passaggio,[3] N. Pastrone,[7] C. Patrignani,[3] J. Peoples, Jr.,[1] F. Petrucci,[2] M.G. Pia,[3] S. Pordes,[1] P. Rapidis,[1] R. Ray,[5,1] J. Reid,[6] G. Rinaudo,[7] B. Roccuzzo,[7] J. Rosen,[5] A. Santroni,[3] M. Sarmiento,[5] M. Savrié,[2] J. Schultz,[4] K.K. Seth,[5] A. Smith,[4] G.A. Smith,[6] M. Sozzi,[7] S. Trokenheim,[5] M.F. Weber,[4] S. Werkema,[1] Y. Zhang,[6] J. Zhao,[5] and G. Zioulas[4]

(Fermilab E760 Collaboration)

[1]*Fermi National Accelerator Laboratory, Batavia, Illinois 60510*
[2]*Istituto Nazionale di Fisica Nucleare and University of Ferrara, 44100 Ferrara, Italy*
[3]*Istituto Nazionale di Fisica Nucleare and University of Genoa, 16146 Genoa, Italy*
[4]*University of California at Irvine, Irvine, California 92717*
[5]*Northwestern University, Evanston, Illinois 60208*
[6]*Pennsylvania State University, University Park, Pennsylvania 16802*
[7]*Istituto Nazionale di Fisica Nucleare and University of Turin, 10125 Turin, Italy*

(Received 20 April 1995)

The E760 Collaboration performed an experiment in the Antiproton Accumulator at Fermilab to study the two photon decay of the $\eta_c(1\,^1S_0)$ charmonium state formed in $\bar{p}p$ annihilations. This resulted in a new measurement of the mass $M_{\eta_c} = 2988.3^{+3.3}_{-3.1}$ MeV/c^2 and of the product $B(\eta_c \to \bar{p}p) \times \Gamma(\eta_c \to \gamma\gamma) = (8.1^{+2.9}_{-2.0})$ eV. We performed a search for the process $\bar{p}p \to \eta_c'(2^1S_0) \to \gamma\gamma$ over a limited range of center-of-mass energies. Since no signal was observed, we derived upper limits on the product of branching ratios $B(\eta_c' \to \bar{p}p) \times B(\eta_c' \to \gamma\gamma)$ in the center-of-mass energy range $3584 \leq \sqrt{s} \leq 3624$ MeV. We observed no signal for the nonresonant process $\bar{p} + p \to \gamma + \gamma$ and obtain upper limits.

PACS number(s): 13.20.Gd, 13.40.Hq, 13.75.Cs, 14.40.Gx

I. INTRODUCTION

The properties of the charmonium ground state $\eta_c(1\,^1S_0)$ and of its first radial excitation $\eta_c'(2^1S_0)$ are of great interest but have not yet been well determined. One reason for this is that $^1S_0$ states have quantum numbers $J^{PC} = 0^{-+}$ and cannot therefore be formed directly in e^+e^- annihilations.

The Mark II Collaboration first detected the η_c at the SLAC storage ring SPEAR by reconstructing the hadronic final states in the radiative decay of the ψ' [1]. This discovery was immediately confirmed by the Crystal Ball Collaboration [2] by studying the inclusive photon spectrum from the reactions

$$e^+ + e^- \to \psi' \to \gamma + \text{anything}\ , \tag{1}$$

$$e^+ + e^- \to \psi \to \gamma + \text{anything}\ , \tag{2}$$

and later by several other experiments performed at e^+e^- colliders reconstructing the hadronic final states in the radiative decay of the ψ [3] (reaction 2) and in the process [4–9]

$$e^+ + e^- \to e^+ + e^- + \eta_c \to e^+ + e^- + \text{hadrons}\ , \tag{3}$$

where the η_c is formed by the fusion of two quasireal photons emitted by the initial e^+e^- pair.

The Crystal Ball Collaboration [10] reported the observation of a peak in the inclusive photon spectrum of ψ' decays in reaction (1) at an energy corresponding to a recoiling state of mass 3594 MeV/c^2. It was interpreted as the first evidence of the η_c'. This state has not been observed in any subsequent experiment.

In all these experiments the precision of the determination of the mass and total width of the charmonium state depends on the resolution of the detector.

In our experiment we studied the reactions

$$\bar{p} + p \to \eta_c(1\,^1S_0) \to \gamma + \gamma\ , \tag{4}$$

$$\bar{p} + p \to \eta_c'(2\,^1S_0) \to \gamma + \gamma\ . \tag{5}$$

 ©1995 The American Physical Society

In $\bar{p}p$ annihilations the $^1S_0$ states can be formed directly through an intermediate state of two gluons, and the parameters of the resonance can be extracted from the excitation profile. The precision of the measurement of the resonance parameters depends only upon our knowledge of the energy of the initial state, provided statistics is not a limiting factor. The initial state energy can be determined to high accuracy by a method, used in this experiment, in which antiprotons of well-known momentum circulating inside a storage ring annihilate on the protons of an internal hydrogen jet target. An excitation curve is obtained by stepping the beam momentum to perform an energy scan across the resonance.[1]

There are two advantages in identifying the formation of $^1S_0$ resonances by detecting the two-photon final state: First, this annihilation process is of great theoretical interest, and second, it is easier to extract the events of interest from the large background of conventional hadronic processes by selecting an electromagnetic final state. Unfortunately, the two photon branching ratios are small (of order 10^{-4}) and the residual background from $\pi^0\pi^0$ and $\pi^0\gamma$ final states is bothersome.

While the technique used in this experiment provided an adequate instantaneous luminosity, ranging typically from 3×10^{30} cm^{-2} sec^{-1} to 10^{31} cm^{-2} sec^{-1}, the integrated luminosity spent at the η_c was limited. Even so, we determined the mass of the resonance with fair statistical accuracy and with negligible systematic uncertainty. The value obtained disagrees with the accepted one [12] and leads to a shift in the value of the hyperfine splitting for the S-wave charmonium ground state, a quantity which is important for the understanding of $q\bar{q}$ spin-spin forces.

We also measured with good precision the product $B(\eta_c \to \bar{p}p) \times \Gamma(\eta_c \to \gamma\gamma)$. We obtained [using $B(\eta_c \to \bar{p}p)$ as determined by other experiments [12]] a value for $\Gamma(\eta_c \to \gamma\gamma)$ that is consistent with theory and with the results of recent experiments that study reaction (3).

We searched for the η_c' over a limited energy interval which includes the region in which the η_c' was originally observed [10]. We did not observe a signal and we report upper limits on the cross section for reaction (5).

II. EXPERIMENTAL METHOD

A. Technique

Experiment E760 was carried out at the Antiproton Accumulator of the Fermilab Antiproton Source and has been described in earlier publications [14]. Up to 5×10^{11} $\bar{p}$ per fill were stored and stochastically cooled in the accumulator ring at the design kinetic energy of 8.0 GeV. The beam was then decelerated to the resonance formation energy. For the η_c this implied crossing the machine transition energy, which was done with lower currents ($\leq 2 \times 10^{11}$ $\bar{p}$) to reduce the risk of losing the beam. Once the antiprotons reached the selected energy, the hydrogen gas jet [15] was turned on and data taking was started. Both the beam and the jet were operated in dc mode and the antiprotons crossed the 3.5×10^{13} atoms/cm^2 hydrogen gas-jet target with a revolution frequency of about 0.6 MHz. The target thickness was large enough to yield a high instantaneous luminosity, but sufficiently small to ensure that the energy loss and multiple scattering of antiprotons traversing it could be continuously compensated for by the accumulator stochastic cooling system. The size of the interaction region was determined transversely by the beam size, $\sim$ 5 mm diameter, and longitudinally by the gas-jet size, $\sim$ 6 mm. Both figures correspond to 95% containment.

To maximize the integrated luminosity, data were taken for about one beam lifetime (40–90 h, depending on the energy) before dumping the beam. The scan of the resonances was performed by accumulating data at a fixed energy for each fill. This corresponded to an integrated luminosity for each energy point of a few hundred nb^{-1} at the η_c and of $\sim$ 1 pb^{-1} at the η_c'. At each energy point we recorded, along with the candidate events, the integrated luminosity value (see Sec. II C) and characteristics of the antiproton beam (such as the revolution frequency spectrum and the orbit position) necessary to reconstruct the beam momentum distribution. By measuring the event yield for the reactions of interest as a function of the center-of-mass energy, an excitation profile was obtained from which the resonance parameters could be extracted. This, in principle, requires that the center-of-mass energy spectrum be deconvoluted from the measured profile to obtain the intrinsic resonance shape. No unfolding was needed for the $^1S_0$ charmonium resonances, as they are expected to have total widths (5 MeV or more) much larger than the spread in the center-of-mass energy in this experiment ($\sim$ 0.5 MeV full width at half maximum).

The mass of the resonance was directly obtained from the energy of the peak of the excitation curve. The precision of the measurement was limited by the statistical error in the peak position; compared to that error, the systematic uncertainty on the center-of-mass energy ($\leq$ 100 keV) [14] was negligible. The resonance total width was determined from the shape of the excitation curve, and the cross section at the resonance peak directly measured the product of branching ratios into the initial and final states, $B(R \to \bar{p}p) \times B(R \to \gamma\gamma)$. Finally, a measurement of the area under the excitation curve yielded the product $\Gamma_R \times B(R \to \bar{p}p) \times B(R \to \gamma\gamma) = \Gamma_{\gamma\gamma} \times B(R \to \bar{p}p)$. The precision of the measurement of the peak cross section and of the total area depends on an accurate determination of the detection efficiency and luminosity; all the measured quantities are sensitive to the subtraction of background which must be measured in nearby control regions. The resolution of the detector does not directly affect the measurement of the resonance parameters and is only relevant for the rejection of background.

[1]This method was pioneered by experiment R704 at the CERN Intersecting Storage Rings (ISR) [11].

B. Data collection

A total integrated luminosity of 3.56 pb^{-1} was collected in the center-of-mass energy range $2910 \leq \sqrt{s} \leq 3100$ MeV to search for evidence of η_c formation. Of the 11 data points taken, 7 were spaced at energy intervals of 3–5 MeV around the resonance mass region $2975 \leq \sqrt{s} \leq 3005$ MeV and 4 were taken away from the resonance to measure the background level. Energy settings and integrated luminosities for all data points are given in columns 1 and 2 of Table I.

The running time allotted to the E760 experiment was insufficient to perform a systematic search for the η_c' over an energy interval wide enough to cover the range of predictions for its mass, with enough luminosity to achieve the required sensitivity. We therefore proceeded to search for the η_c', taking data at center-of-mass energies compatible with the mass value of the Crystal Ball η_c' candidate [10], and in one of the ranges ($3612 \leq \sqrt{s} \leq 3620$ MeV) favored by theory [16]. To estimate the background level at these energies we used four more data points, at $\sqrt{s}$ = 3524.0, 3526.0, 3686.0, and 3667.7 MeV. The first three were taken during energy scans of the $h_c(^1P_1)$ and ψ' resonances (which cannot decay into a $\gamma\gamma$ final state). The data from the $h_c(^1P_1)$ scan were divided in two parts, corresponding to data taken on and off resonance. As expected, the cross section for $\gamma\gamma$ candidates was consistent for the two sets of data. Energy settings and integrated luminosities for the ten points are listed in columns 1 and 2 of Table II.

C. Luminosity measurement

The integrated luminosity for each energy setting was obtained by counting the number of recoil protons from $\bar{p}p$ elastic scattering in a silicon detector located at 86.5° from the beam direction. The absolute luminosity was extracted using the known $\bar{p}p$ total cross section [17], the solid angle subtended by the detector, and the detector efficiency which was close to unity. The error in the measurement from counting statistics and background subtraction was $\sim$ 0.5%. The systematic error includes a contribution from the total cross section which is known to $\sim$ 1.0% in this energy range and from the detector solid angle which was determined [18] by using a ^{241}Am standard α source whose activity was calibrated by the U.S. National Bureau of Standards to ±0.43%. Addition of the systematic errors in quadrature yields ±2.1%. Based on these considerations, we conservatively assigned an error of $\sim$ 4% to the absolute luminosity value.

TABLE I. Summary of data for the η_c scan.

$\sqrt{s}$ (MeV)	$\int \mathcal{L}dt$ (nb^{-1})	Events $\lvert\cos\theta_\gamma^*\rvert \leq 0.25$	Cross section $\lvert\cos\theta_\gamma^*\rvert \leq 0.25$ (pb)
2911.3	53.1	2	$60.9\ ^{+80.3}_{-39.3}$
2950.1	197.5	17	$139.1\ ^{+42.5}_{-33.5}$
2974.9	423.9	27	102.9 ± 14.3
2979.2	165.3	11	$107.5\ ^{+43.1}_{-31.9}$
2981.2	392.6	40	164.6 ± 26.0
2985.5	200.2	12	$96.9\ ^{+37.0}_{-30.5}$
2989.6	513.0	47	148.0 ± 21.6
2994.0	308.9	27	141.3 ± 27.2
3005.0	511.0	26	82.2 ± 16.1
3049.7	120.0	2	$26.9\ ^{+35.4}_{-17.3}$
3096.9	626.0	11	$28.4\ ^{+11.3}_{-8.4}$

TABLE II. Summary of data for the η_c' search.

$\sqrt{s}$ (MeV)	$\int \mathcal{L}dt$ (pb^{-1})	Events $\lvert\cos\theta_\gamma^*\rvert \leq 0.4$	Cross section $\lvert\cos\theta_\gamma^*\rvert \leq 0.4$ (pb)
3524.0	6.610	65	18.3 ± 2.3
3526.1	9.389	86	17.1 ± 1.8
3590.8	0.924	4	$8.1^{+6.4}_{-3.9}$
3594.6	0.827	7	$15.8^{+8.5}_{-5.8}$
3612.8	1.167	2	$3.2^{+4.2}_{-2.1}$
3615.9	1.276	9	$13.1^{+6.0}_{-4.3}$
3618.9	0.575	4	$13.0^{+10.3}_{-6.2}$
3621.1	1.216	12	$18.4^{+7.0}_{-5.2}$
3667.7	0.372	2	$10.0^{+13.1}_{-6.5}$
3686.0	0.995	7	$13.1^{+7.0}_{-4.8}$

D. Detector

The E760 detector, shown in Fig. 1, was a nonmagnetic spectrometer with cylindrical symmetry about the beam axis [14], optimized for the identification of charmonium states decaying to e^+e^- or $\gamma\gamma$ and of multi-γ final states. It covered the entire azimuth (ϕ) and the polar angle (θ) from 2° to 70°. It consisted of three sets of scintillator hodoscopes, two in the central region (H1, H2) and one in the forward region (FCH), a multicell threshold gas Čerenkov counter for electron identification, several layers of charged tracking detectors, and two electromagnetic calorimeters, the forward calorimeter and the central calorimeter covering the regions $2° \leq \theta \leq 11°$ and $11° \leq \theta \leq 70°$, respectively.

The detector element that was essential for identifying the $\gamma\gamma$ final state was the central electromagnetic calorimeter [19]. It had to distinguish between $\bar{p}p \to \gamma\gamma$ events and the large background from processes such as $\bar{p}p \to \pi^0\pi^0$ and $\bar{p}p \to \pi^0\gamma$, which have cross sections up to 10^3 times larger than those of reactions (4) and (5). Rejection of these backgrounds requires a granularity adequate to identify the two photons from symmetric π^0 decays, and a low-energy threshold to detect the low-energy photons from highly asymmetric π^0 decays.[2] The central calorimeter consisted of 1280 (64 in ϕ by 20 in θ) lead glass Čerenkov counters pointing to the beam-jet

[2]Symmetric refers to decays where the two photons have similar energies and therefore a nearly minimum opening angle; highly asymmetric refers to decays where one of the photon takes almost all the energy of the parent π^0.

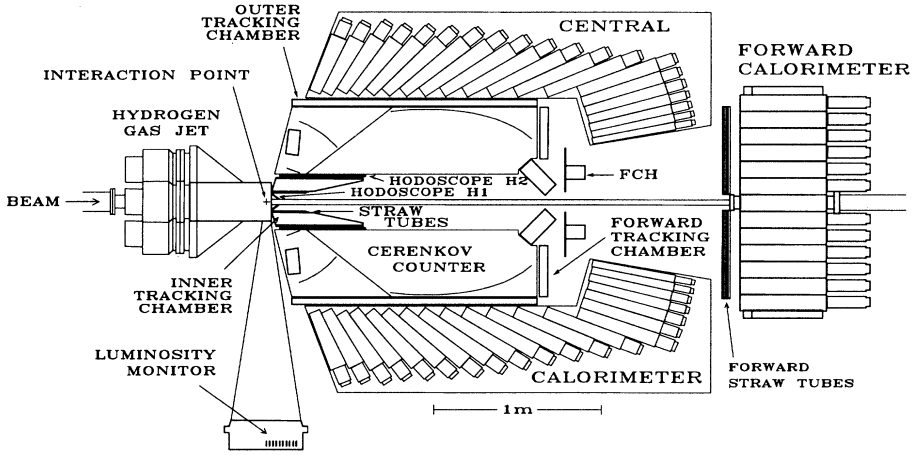

FIG. 1. E760 detector layout.

interaction region. The average rms energy resolution was $\sigma_E/E = 6.0\%/\sqrt{E(\mathrm{GeV})} + 1.4\%$. The average rms error on the reconstructed centroid of an electromagnetic shower was 9 mm, which combined with the uncertainty in the interaction point to give an angular resolution of 6 mrad in θ and 11 mrad in ϕ. The calibration of these counters was obtained *in situ* using both $\bar{p}p \to \psi \to e^+e^-$ and $\bar{p}p \to \pi^0\pi^0$ events.

E. Trigger

The total $\bar{p}p$ cross section is as large as 70 mb in the energy region of interest, corresponding to an interaction rate of about 700 kHz at the experiment peak luminosity of $\sim 10^{31}$ cm^{-2} sec^{-1}.

Events of interest were selected by a fast hardware trigger (level 1), and then transferred to a set of processors where a software filter (level 2) was applied before recording the events on tape. The level 1 trigger accepted in parallel (a) final states containing a large mass object decaying either into an e^+e^- pair (a1) or into two photons (a2), (b) all neutral final states where $\geq 80\%$ of the event energy was contained in the central calorimeter, (c) a sample of events containing only two charged particles consistent with two-body kinematics, and (d) a sample of minimum bias events.

The element common to the (a1) and (a2) triggers was a topological requirement on the electromagnetic showers in the central calorimeter (PBG1), tailored to accept high-mass two-body final states with full efficiency. This required the presence of two showers with energy above a θ-dependent threshold and approximately coplanar with the $\bar{p}$ direction. It was implemented as follows [20]. To reduce the number of signals to a manageable level, the analog signals from the individual counters were summed to produce a matrix of 40 supermodules (8 in ϕ by 5 in θ). The reduction, from 1280 to 160 signals, and then from 160 to 40, was performed in two successive stages. In the first, signals from groups of 9 adjacent counters (same θ) were added to form 8 octants, with one counter overlap, for each of the 20 θ values. In the second, the resulting 160 signals (8 in ϕ by 20 in θ) were summed over θ in groups of 5, again allowing a one counter overlap. The 40 analog signals from the supermodules were integrated and discriminated. The thresholds were set to select events loosely satisfying the two-body decay kinematics of a charmonium state, and were adjusted to the appropriate values for each state measured. A logical OR was constructed of the discriminator outputs from the 5 supermodules in each octant to form the 8 logic signals used for triggering. PBG1 required that two of these signals came from opposing octants (1 against 3) to impose a rough coplanarity.

The trigger rate for the e^+e^- (a1) final state was further reduced to ≤ 20 Hz at peak luminosity by requiring a threefold coincidence between corresponding (consistent ϕ) elements of the H1, H2 hodoscopes and of the Čerenkov counter. Given the small rate, no filtering at level 2 was necessary for this class of events which were all recorded on tape.

To select events of type (a2), it was required that no charged particles be detected in the final state, a condition implemented by vetoing, on signals from H1 or FCH, which together fully covered the polar angle range $2^\circ \leq \theta \leq 65^\circ$ over the complete azimuth. With this requirement the level-1 trigger rate for (a2) was ≤ 50 Hz. The level-1 trigger rate for (b) was ≤ 700 Hz. The level-1 trigger logic required a total time of about 350 ns, and the event readout from the CAMAC front end took about 100 μsec, resulting in a $\sim 90\%$ live time.

The software trigger was performed by 26 Fermilab ACP [21] processors, whose main tasks were to convert the recorded pulse heights to energies, to reconstruct shower positions and energies, and to calculate the invariant mass of all candidate photon pairs. The clustering algorithm used in the ACP was a simplified version of the one used in the off-line analysis (to be described later). For the type of events considered here, the typical processing time per node was ~ 5 msec. Events with a two-cluster invariant mass ≥ 2.0 GeV/c^2, or with the total calorimeter energy $\geq 90\%$ of the available energy, were written on tape. The level-2 filter rejected $\sim 80\%$ of the level-1 triggers of type (b). The data summary tapes (DST's) used for the $\gamma\gamma$ analysis contained events with ≤ 5 calorimeter clusters.

F. Trigger efficiency for $\gamma\gamma$ events

To determine the absolute cross sections, we estimated the efficiency of the PBG1 requirement and the loss from the charged particle veto. The PBG1 efficiency was determined from a sample of events of the type

$$\bar{p}p \to \psi \to e^+e^- \tag{6}$$

collected at the ψ formation energy. The rate for this reaction was sufficiently large that a background-free sample of ~ 3500 events could be extracted without requiring PBG1 in the trigger. Since the PBG1 "bit" was found to be set in all the events of this sample, we concluded that the PBG1 requirement was fully efficient.

The same ψ events were used to measure the efficiency of the level-2 filter for the events of type (a2). This was possible because the calorimeter response to events with an e^+e^- final state was indistinguishable from its response to events with two photons. Applying *a posteriori* the filtering program to the ψ sample we found that no events were rejected, implying that the level-2 filter was also fully efficient.

A sample of data was taken at $\sqrt{s} = 3.1$ GeV at a luminosity of 3.5×10^{30} cm^{-2} sec^{-1}, with a special trigger that did not have an all neutral requirement but demanded only that at least 85% of the total energy be deposited in the central calorimeter. These data were subjected to the PBG1 requirement at the software level. A background-free sample of $\pi^0\pi^0$ events was selected with a kinematical fit and mass cuts on the reconstructed pions. We were then able to measure the inefficiency introduced by the veto requirement on H1 and FCH. We found that 13.1% of the events had either the H1 or FCH trigger bit set. Subtracting the contributions from Dalitz decays (1.2% for each π^0) and photon conversions in the beam pipe (1.1% per photon), the loss from accidentals was found to be $(13.1-2.4-4.4)\% = 6.3\%$. This implies an inefficiency for the $\gamma\gamma$ final state of 8.5% (6.3% from accidentals and 2.2% from either photon converting in the beam pipe).

The dominant source of accidentals was δ rays produced by the antiproton beam in the target; hence, the accidental rate was luminosity and energy dependent. This dependence was studied [22] by measuring the rate of extra-hits in H1 and FCH in $\bar{p}p \to \psi \to e^+e^-$, $\bar{p}p \to \chi_{1,2} \to \psi + \gamma \to e^+e^- + \gamma$, and $\bar{p}p \to \psi' \to e^+e^-$ events from data samples taken at different instantaneous luminosities. The accidental rate was found to increase linearly with the event rate and the fit to these data was used to scale the inefficiency determined from a $\pi^0\pi^0$ data sample (as described above) to the value appropriate for the average event rate of each energy point. For data taken at $2911 \le \sqrt{s} \le 3097$ MeV, the average trigger efficiency was $(91 \pm 2)\%$, with no more than 2% variation between energy points. Similarly, for data taken at $3524 \le \sqrt{s} \le 3686$ MeV, the average trigger efficiency was $(88 \pm 3)\%$.

G. Event pileup

The first level trigger initiated the analog-to-digital conversion of signals from the individual calorimeter counters and the triggering hodoscopes. The gate for the central calorimeter signals was 150 ns wide, to allow for the tails induced by the long delay cables. At the highest luminosities, as used for the η_c' search, pulse tails associated with earlier events often resulted in extra pulses in the calorimeter data. Since the experiment analysis was designed to identify specific event topologies, these could lead to the rejection of valid events. A partial solution was achieved by two artifices that provided information to identify in-time electromagnetic showers in the off-line analysis. In one, the 160 outputs from the first stage of summing were discriminated (threshold set at an equivalent energy of $\sim$ 40 MeV) and read out with latches set with a 30 ns gate. In the other, the signals from the 40 supermodules were recorded in two separate sets of analog-to-digital converters (ADC's), one with normal timing and the other, designed to identify energy deposits from out-of-time events, with the signals delayed by 50 ns and a gate 100 ns long. The use of this information is described below.

III. ANALYSIS

A. Shower analysis

1. Pattern recognition

The algorithm for shower reconstruction in the central calorimeter [23] searched for local maxima (counters with more energy than their eight nearest neighbors) and formed 3×3 clusters around these. Energy thresholds of 5 MeV for the central counter and 20 MeV for the entire nine-counter cluster were used. The transverse coordinate of the shower centroid was determined in two steps: In the first, the energy-weighted center of gravity of the cluster was determined. This first approximation to the shower position was in general closer to the center of the highest-energy lead-glass counter than the true position was. The calculation of the centroid coordinates was improved in the next step by parametrizing the transverse shower profile as the sum of two exponentials describing the core and the diffuse part of the shower, respectively. The two slope parameters were determined empirically from data collected in a calibration run at an external beam with electrons in the 1–4 GeV energy range [19] and from the study of electrons from ψ decays .

When two clusters overlapped, the energies of the counters (from one to three counters) in the overlap region were shared using an iterative procedure. The parametrization of the transverse shower profile was used to determine the fraction of each counter energy to be assigned to each cluster. At each iteration, new energies and new positions were determined and compared to the energies and positions of the previous step. The process was stopped when the cluster centroids and energies were stable within the intrinsic detector resolution. Convergence was normally reached in two to three iterations.

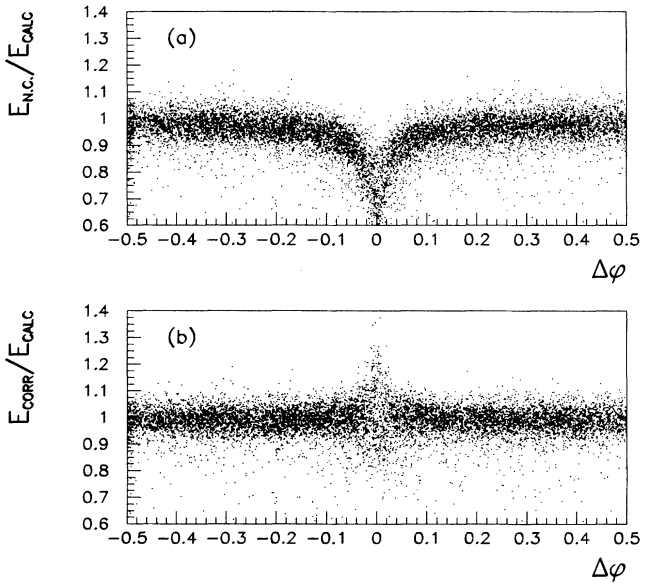

FIG. 2. Ratio of measured to calculated shower energy as a function of the azimuthal distance, in block units, from the shower centroid to the nearest crack between two lead glass counters: (a) before correction, (b) after correction.

2. *Energy corrections*

The support structure of the central calorimeter modules introduced a small amount of passive material (referred to as cracks) between neighboring counters (1.46 mm stainless steel between counters adjacent in ϕ, and 0.25 mm between counters adjacent in θ). This represented only 2.8% of the surface area of the detector, as seen by the incoming photons. However, for a photon impinging near (or in) a crack a non-negligible fraction of the energy was released in the passive material and escaped detection. Therefore, a correction was applied to the energy of the shower; this correction was a function of the photon impact point with respect to the central counter edges. The correction function was derived from the data of the test-beam run and the parameters were set using electron showers from $\psi \to e^+e^-$ decays. Figure 2 shows the ratio $E_{\rm meas}/E_{\rm calc}$ as a function of the azimuthal distance, in block units, from the shower centroid to the nearest crack, for electrons from $\bar{p}p \to \psi \to e^+e^-$, before and after the correction was applied. $E_{\rm calc}$ is the electron energy calculated from the measured polar angles using two-body kinematics. At the counter edges the correction was as much as 45%. It should be noted that this variation in the calorimeter response did not affect the trigger efficiency as demonstrated by the fact that the measured PBG1 efficiency was $\sim 100\%$.

3. π^0 *identification*

The major sources of background to the $\gamma\gamma$ signal were $\pi^0\pi^0$ and $\pi^0\gamma$ events in which the π^0 decay was either nearly symmetric or highly asymmetric. A symmetric decay produced a pattern of energy deposits that could be mistaken for a single photon shower since for high-energy pions the separation between photons was as small as 1.5 block widths. In order to identify such cases, an effective mass was calculated for each cluster:

$$m_{\rm cluster} = \sqrt{\left(\sum_i E_i\right)^2 - \left(\sum_i \vec{p_i}\right)^2}\,, \qquad (7)$$

where E_i is the energy deposited in the ith counter of the cluster, $\vec{p_i} = E_i\hat{r_i}$, and $\hat{r_i}$ is the unit vector from the interaction point to the center of the ith counter. The sums are for a 5×5 array of counters about the cluster centroid. Clusters from symmetric π^0 decays have large $m_{\rm cluster}$ values, while those from single photons (or electrons) do not. Figure 3 shows the $m_{\rm cluster}$ distributions for showers from ψ electrons and for showers inter-

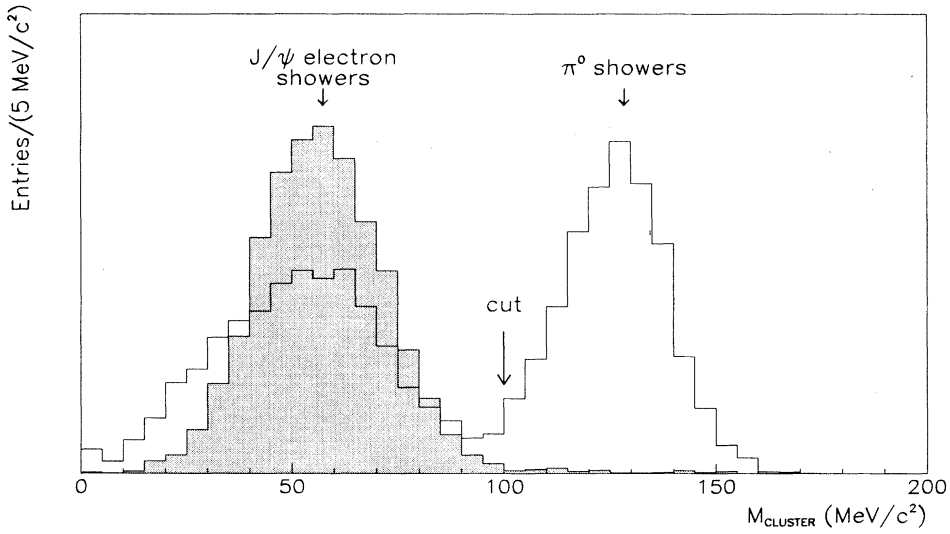

FIG. 3. Distributions in the $m_{\rm cluster}$ variable used to identify π^0 decays with coalescing gammas.

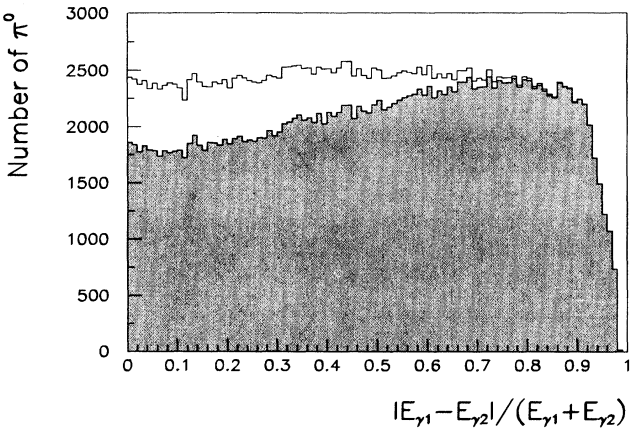

FIG. 4. Energy asymmetry in π^0 decays. The open histogram includes π^0's resolved by cluster splitting, while the shaded one does not.

preted as coalescing π^0's. The latter are obtained from three-cluster events fitting the two-body kinematics of $\bar{p}p \to \pi^0\pi^0$, where the other two clusters (not entering the histogram) reconstruct to give a π^0. The low $m_{\rm cluster}$ showers from the $\pi^0\pi^0$ sample in Fig. 3 were due to isolated photons either from large opening-angle asymmetric π^0 decays (where the low energy photon was not detected) or from $\bar{p}p \to \pi^0\gamma$ events.

Any cluster with $m_{\rm cluster} \geq 100$ MeV/c^2 was split into 2, each part representing an individual photon from the π^0. The identification of symmetric π^0 decays based on the $m_{\rm cluster}$ cut was estimated to be more than 99% efficient. This is demonstrated in Fig. 4 which shows the energy asymmetry of photons from π^0 decay. The shaded histogram shows the distribution of π^0 decaying into two distinct clusters; the open histogram also contains π^0s whose decay γ's were derived by splitting a cluster. The final distribution is nearly uniform, with a small loss of highly asymmetric decays where a low-energy photon was lost because either it was emitted outside the acceptance or its energy fell below the calorimeter threshold. $\pi^0\pi^0$ and $\pi^0\gamma$ final states where the π^0's decay asymmetrically constituted the most severe background to reactions (4) and (5).

4. Timing analysis

To conclude the discussion of shower analysis we describe the technique adopted to tag in-time clusters. As mentioned in Sec. II G, when running at the highest instantaneous luminosities, we experienced a substantial pileup problem in the calorimeter data. As an example, when running at a center-of-mass energy of 3525 MeV with $\mathcal{L} = 0.7 \times 10^{31}$ cm^{-2} sec^{-1}, one out of four events had at least one cluster from an out-of-time interaction, with an average of 1.5 such clusters per event. Whether a cluster was in time or out of time was determined by comparing the ADC counts generated by the prompt and delayed signals from the 40 supermodules, or from the status of the latches connected to the 160 outputs of the first level summers (see Sec. II G). When a supermodule was populated with only one cluster, the ratio R of the delayed to the prompt ADC outputs of the supermodule was examined. Signals appearing earlier than the trigger had unusually large values of R, while signals arriving later than the trigger had small values. When R was within the appropriate intermediate range, a cluster was identified as in time, while an R value outside this range resulted in an out-of-time identification for the cluster. When more than one cluster was present in a supermodule, the ratio R was used for any cluster that contributed more than 75% to the supermodule output; otherwise, the status of the latches described in Sec. II G was examined. A cluster was identified as in time if an appropriate latch was set and no other clusters contributed to the first-level summer output. If a cluster contribution to a first-level summer output was greater than the latch threshold and the latch was not set, then the cluster was determined to be out of time. The cluster time was undetermined if the contribution to the first-level summer output by the cluster was below the latching threshold, or if more than one cluster contributed to the same first-level summer output.

The performance of the timing algorithm was studied using a sample of well identified $\bar{p}p \to \pi^0\pi^0$ events, selected with a tight kinematic fit and with no limit on the presence of low-energy (< 200 MeV) extra clusters. It was found that the four photon showers belonging to the event were classified without mistake (i.e., in time or undetermined) when their energy was above ~ 100 MeV, whereas, for instance, at 50 MeV, 13% of the valid photons were incorrectly classified as out of time. In this sample, taken at an average luminosity of 0.7×10^{31} cm^{-2} sec^{-1}, only $\sim 3\%$ of the events had an accidental cluster of energy greater than 120 MeV that was identified as in time.

B. Event selection

To select $\gamma\gamma$ candidates with high efficiency while reducing the background from $\pi^0\pi^0$ and $\pi^0\gamma$ final states to an acceptable level, it was crucial to reliably tag in-time clusters and to identify and reject asymmetrically decaying π^0's. After reconstruction, we tagged each cluster by applying the algorithms described in Sec. III A, except when dealing with clusters of energy ≤ 100 MeV, which we always identified as undetermined. The events accepted had exactly two in-time clusters (of $E_{\rm cluster} \geq 100$ MeV) and any number of out-of-time or undetermined clusters in the central calorimeter and no clusters in the forward calorimeter, where most of the background channels contributed photons. We required that the two in-time clusters give a reconstructed invariant mass $M_{\gamma\gamma} \geq 2.5$ GeV/c^2.

To reduce the background from events with π^0's decaying asymmetrically to a high-energy (in-time) photon and a low-energy one classified as undetermined, invariant mass values were also calculated by pairing any undetermined extra cluster with each of the two high-energy clusters. A plot of the resulting invariant mass ($M_{\rm pair}$) distribution is given in Fig. 5. Events contributing to the

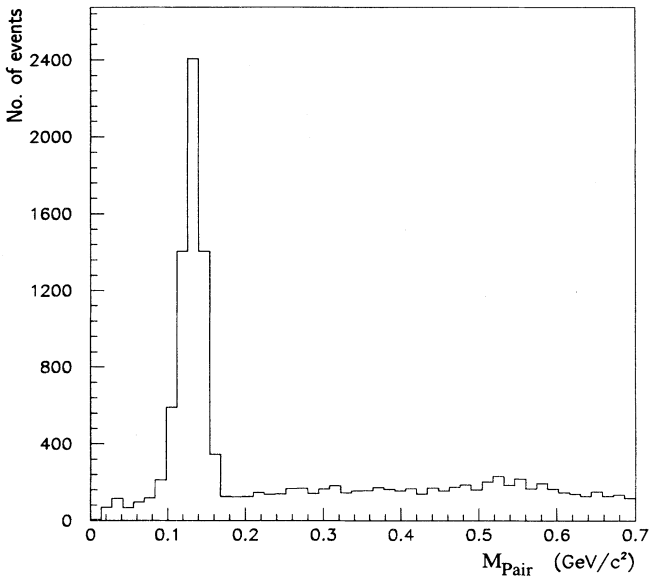

FIG. 5. Invariant mass reconstructed combining each of the two in-time clusters of a $\gamma\gamma$ candidate event with any of the undetermined extra clusters present in the same event.

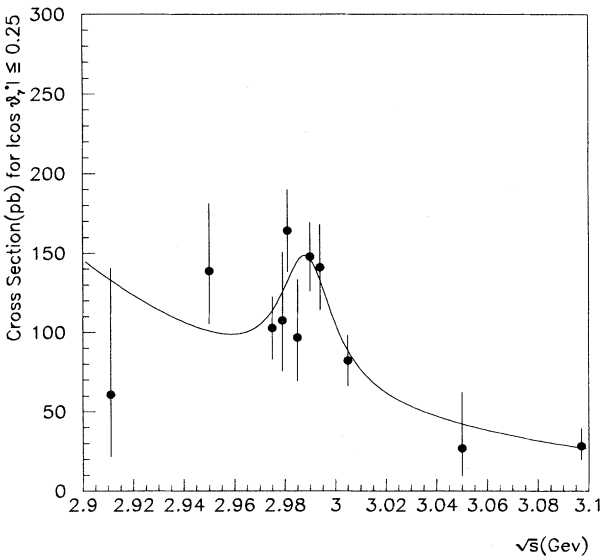

FIG. 6. Measured cross section for $\bar{p}p \to \gamma\gamma$, in the η_c energy region. The line represents the best fit to the data. The choice of the acceptance cut $[|\cos(\theta_\gamma^*)| \leq 0.25]$ and fitting procedure are explained in Sec. IV C.

large peak in the π^0 mass region (80 MeV$\leq M_{\rm pair} \leq$200 MeV) were removed. Finally, a four constraint (4C) kinematical fit to the $\gamma\gamma$ hypothesis was applied to the remaining sample, and events with a nominal χ^2 probability ≤ 0.1 were rejected. Since χ^2 departs from the usual distribution due to the complexity of the measurement errors in these data, the efficiency of the associated probability cut is less than 0.9 and is estimated from data as described below.

The analysis efficiency was measured from background-free samples of $\bar{p}p \to \psi \to e^+e^-$ and $\bar{p}p \to \psi' \to e^+e^-$ events, selected using only the information from the hodoscopes and the Čerenkov counter. As mentioned above, these events were indistinguishable from $\gamma\gamma$ events in the calorimeter. The efficiencies calculated from ψ and from ψ' samples were $\epsilon_{\rm analysis} = 0.68 \pm 0.01$ and $\epsilon_{\rm analysis} = 0.61 \pm 0.03$, respectively. The comparison of these two values indicates a systematic difference in the two results, which came from samples taken at different beam energies and with different instantaneous luminosities. We therefore applied to the data taken in the η_c region the value of the analysis efficiency obtained from ψ data, which were close in energy and taken at comparable luminosities. Similarly we applied the value of the analysis efficiency obtained from ψ' data to the data taken in the η_c' region.

IV. RESULTS

In Figs. 6 and 7 we plot the measured cross sections as a function of center-of-mass energy for data taken in the energy intervals 2900 MeV $\leq \sqrt{s} \leq$ 3100 MeV and 3520 MeV $\leq \sqrt{s} \leq$ 3690 MeV, respectively.

A structure over a continuum level is visible in each plot. The signal at $\sqrt{s} \sim$ 2990 MeV in Fig. 6 is attributed to the process $\bar{p}p \to \eta_c \to \gamma\gamma$ while that at $\sqrt{s} \sim$ 3556 MeV in Fig. 7 comes from the process $\bar{p}p \to \chi_2 \to \gamma\gamma$ and has been discussed elsewhere [24]. The observed continuum, which decreases with center-of-mass energy, is the sum of a background component (referred to in what follows as "feed-down") from events with n γ's in the final state where $(n-2)$ γ's are not detected and where the remaining two γ's mimic a two-

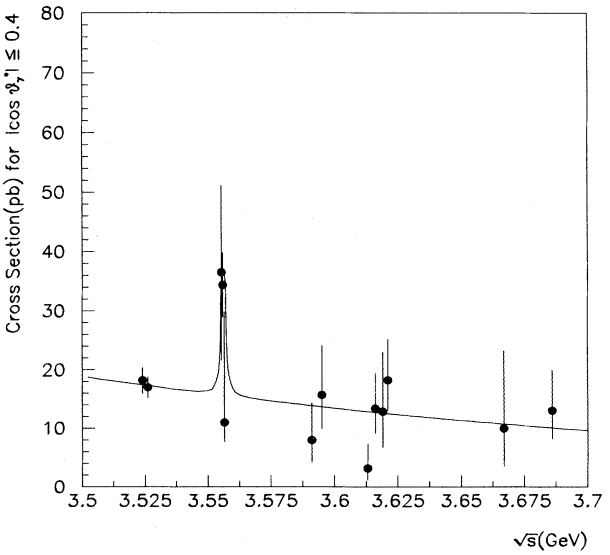

FIG. 7. Measured cross section for $\bar{p}p \to \gamma\gamma$. The line represents the best fit to the data. In this fit the mass and total width of the χ_2 resonance were fixed to the values determined in Ref. [14]. The choice of the acceptance cut $[|\cos(\theta_\gamma^*)| \leq 0.4]$ is explained in Sec. IV D.

body final state, and a component from the electromagnetic process

$$\bar{p} + p \to \gamma + \gamma \ . \tag{8}$$

This last process, interesting in its own right, could in principle lead to interference effects with the resonant channels $\bar{p}p \to (\bar{c}c) \to \gamma\gamma$. It is therefore important to estimate its cross section level.

A. Background study

To understand the feed-down, we studied annihilations into multiple π^0's. Based on our measurement of the $\bar{p}p \to 3\pi^0$ process we estimated the background to the 2γ sample from this and higher multiplicity π^0 final states to be negligible [25]. Contributions from channels with η's and π^0's in the final states were also found to be negligible [25].

The feed-down contribution from the reaction

$$\bar{p} + p \to \pi^0 + \pi^0 \tag{9}$$

was determined by studying events with four or three γ's. Starting with fully reconstructed $\pi^0\pi^0$ events, a simulation was used to determine the background fed into the 2γ sample. The simulation was performed as follows: (a) generation of events from reaction (9) with a flat distribution in $\cos\theta^*_{\pi^0}$ (where $\theta^*_{\pi^0}$ is the angle of emission of the π^0 relative to the $\bar{p}$ direction, in the $\bar{p}p$ center-of-mass system), (b) modeling of the transverse shower distribution of each photon in the final state and calculating the energy deposited in the individual lead-glass counters in the central calorimeter, and (c) reconstruction of the event using the experiment's off-line analysis package and applying the same selection criteria as applied to the data. To reproduce the $\pi^0\pi^0$ angular distribution, data and simulated events were binned in 0.05-wide $\cos\theta^*_{\pi^0}$ intervals. Normalization factors were calculated in each bin as ratios of the numbers of observed and simulated 4γ events. These normalization factors were then used to weight the number of simulated events with two and three photons.

A comparison of the observed 3γ events with the prediction of the simulation revealed a significant excess in the data; we attributed this to the reaction

$$\bar{p} + p \to \pi^0 + \gamma \ , \tag{10}$$

which we therefore included in the background calculation. The feed-down contributions from the $\pi^0\pi^0$ and $\pi^0\gamma$ reactions are comparable.

The feed-down background strongly depends upon the threshold set for detecting low-energy photons in the central calorimeter (20 MeV). The uncertainty in the absolute energy scale for soft photons is the dominant source of systematic error in the estimate of this background (a systematic underestimate of the energy of soft photons by 20% would cause an 8% increase in the feed-down level). A detailed discussion of the background calculations and our results for reactions (9) and (10) are given elsewhere [25].

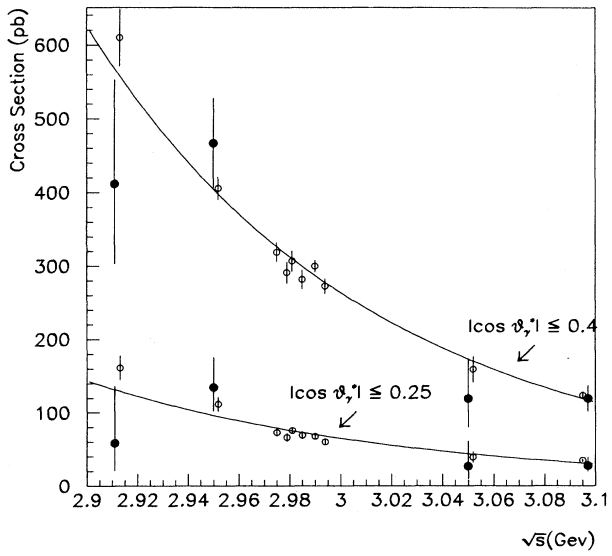

FIG. 8. Cross section in the center-of-mass energy range from 2900 to 3100 MeV for $\bar{p}p \to \gamma\gamma$ candidates. Solid circles represent the data points, while the open circles are estimated feed-down cross sections. The lines are the best fits of the feed-down cross sections using Eq. (11). Data in the vicinity of the η_c resonance at 2990 MeV are removed. The feed-down points are offset in $\sqrt{s}$ for clarity.

B. Nonresonant $\bar{p}p$ annihilation into $\gamma\gamma$

The estimated feed-down background from reactions (9) and (10) is compared to the data (solid circles) in Fig. 8 and Fig. 9.

The acceptance in $|\cos\theta^*_\gamma|$ (where θ^*_γ is the angle of the γ relative to the $\bar{p}$ direction in the $\bar{p}p$ center-of-mass system) is limited to $|\cos\theta^*_\gamma| \leq 0.4$ to avoid edge effects in the lead-glass calorimeter. To make the comparison

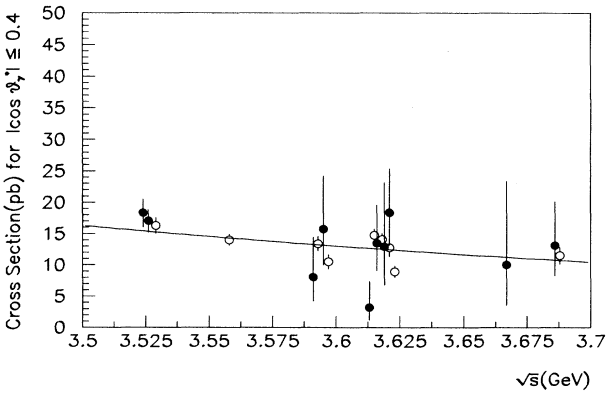

FIG. 9. Cross section in the center-of-mass energy range from 3520 to 3690 MeV for $\bar{p}p \to \gamma\gamma$ candidates with $[|\cos(\theta^*_\gamma)| \leq 0.4]$. Solid circles represent the data points, while the open circles are estimated feed-down cross sections. The line is the best fit of the feed-down cross sections to Eq. (11). Data in the vicinity of the χ_2 resonance at 3556 MeV are removed. The feed-down points are offset in $\sqrt{s}$ for clarity.

TABLE III. Background cross section parameters, for feed-down and for the process $\bar{p}p \to \gamma\gamma$.

$\sqrt{s_0}$ (MeV)	$\cos(\theta^*_\gamma)$ cut	D	B	A[a] (pb)	C[b] (pb)	Upper limit on C (90% C.L.) (pb)
2988	0.25	0.0	24.7 ±5.5	71.5 ± 6.4	0.0 ± 9.9	16.4
	0.25	5.0	24.8 ±5.4	71.4 ± 6.4	0.6 ± 11.2	18.0
	0.25	10.0	24.8 ±5.3	71.2 ± 6.5	1.4 ± 12.2	21.6
2988	0.40	0.0	25.5 ±2.8	292.2 ± 12.9	5.1 ± 19.9	32
	0.40	5.0	25.5 ±2.7	291.9 ± 13.0	6.5 ± 22.6	36.
	0.40	10.0	25.4 ±2.7	291.7 ± 13.1	8.1 ± 25.1	43.
3600	0.40	0.0	11.4 ± 4.5	13.0 ± 1.3	0.5 ± 1.6	2.3
	0.40	5.0	11.3 ±4.4	13.0 ± 1.3	0.5 ± 1.5	2.2
	0.40	10.0	11.2 ±4.3	13.0 ± 1.3	0.5 ± 1.4	2.0

[a] $A = \sigma_{fd}$ at $\sqrt{s_0}$.
[b] $C = \sigma_{\bar{p}p\to\gamma\gamma}$ at $\sqrt{s_0}$.

more obvious we suppress the data points around the resonances. The solid lines represent the fit of the feed-down cross section to a power law

$$\sigma_{\rm FD} = A(\sqrt{s_0}/\sqrt{s})^B \ . \tag{11}$$

The nonresonant electromagnetic process (8) should manifest itself as an excess of events over the calculated background at all energies. No excess is seen in our data either in the η_c energy region or at higher energies, and we set upper limits to the cross section for reaction (8). To extract such limits, we performed a maximum likelihood fit of the data of Fig. 8 and Fig. 9 to a superposition of the process (8) and of the feed-down. The energy dependence of the cross section for reaction (8) was also parametrized with a power law

$$\sigma_{\bar{p}p\to\gamma\gamma} = C(\sqrt{s_0}/\sqrt{s})^D \ . \tag{12}$$

In this fit we fixed the value of the exponent D and determined the values of A, B, and C. C and A are the cross sections at $\sqrt{s_0}$, integrated over the selected angular region, for $\bar{p}p \to \gamma\gamma$ and for the feed-down, respectively. The results of the fit for the two sets of data are reported in Table III. They are calculated for three values of the parameter D. The upper limits (90% C.L.) were derived by normalizing the probability distribution to the physical region ($C \geq 0.0$), following the prescription of the Particle Data Group (Ref. [12], p. 1280). For D=10, which is the value favored by theory [26, 27] and which is consistent with the CLEO data (see below), we find a 90% upper limit of 43 pb for $\sigma_{\bar{p}p\to\gamma\gamma}$ with $|\cos\theta^*_\gamma| \leq 0.4$ at a $\sqrt{s}$ of 2988 MeV. We compare our result to that obtained by the CLEO Collaboration [28], which extracted the cross section for reaction

$$\gamma + \gamma \to \bar{p} + p \tag{13}$$

from measurements of the reaction $e^+e^- \to e^+e^-\bar{p}p$. The cross section CLEO measured is restricted to the angular region $|\cos\theta^*_\gamma| \leq 0.6$. Averaging their data from 2.8 to 3.2 GeV, using their angular distribution to scale down to $|\cos\theta^*| \leq 0.4$, and applying detailed balance, we obtain an estimate from CLEO data of the cross section for reaction (8) at 2988 MeV of $\sim$ 60 pb for $|\cos\theta^*_\gamma| \leq 0.4$, larger than our 90% upper limit of 43 pb.

Theory [26, 27] gives little guidance here since the predictions for $\sigma(\bar{p} + p \to \gamma + \gamma)$ substantially differ and can accomodate both our result and that obtained by CLEO. Hyer [29] has given an estimate of the ratio

$$R = \frac{\sigma(\bar{p} + p \to \gamma + \gamma)}{\sigma(\bar{p} + p \to e^+ + e^-)} \ . \tag{14}$$

which depends only on the quark momentum distributions within the proton. The ratio formed from our result for $\sigma(\bar{p} + p \to \gamma + \gamma)$ and our previously published result for $\sigma(\bar{p} + p \to e^+ + e^-)$ [30] agrees within large errors with Hyer's prediction.

C. Results for the η_c ($1\,^1S_0$)

The angular distributions of the $\gamma\gamma$ candidates for data taken at $\sqrt{s}$ =2950 MeV (a), $\sqrt{s}$ = 2990 MeV (b), and $\sqrt{s}$ = 3097 MeV (c) are shown in Fig. 10. The dashed curves are the results of polynomial fits to the differential feed-down cross sections. The two experimental distributions (a) and (c) agree quite well with the background predictions, while there is an excess of $\gamma\gamma$ candidates in (b) that is consistent with resonance formation at this energy.

The angular distribution of the background is almost constant up to $|\cos\theta^*_\gamma| = 0.2$ and rapidly increasing above this value, while the signal is expected to be flat in $|\cos\theta^*_\gamma|$ for the S-wave η_c resonance. It is therefore desirable to limit the acceptance to small values of $|\cos\theta^*_\gamma|$. The significance of the signal will vary with the cut on $|\cos\theta^*_\gamma|$. Moving the cut upwards through the flat region enriches the statistics at constant signal-to-background ratio, thus making the significance rise. When the cut is moved farther into the region of rising background, the ratio of signal to background becomes less and less favorable, and the significance decreases after going through a shallow maximum. By using the differential cross section for the feed-down and a signal level within a plausible range, we

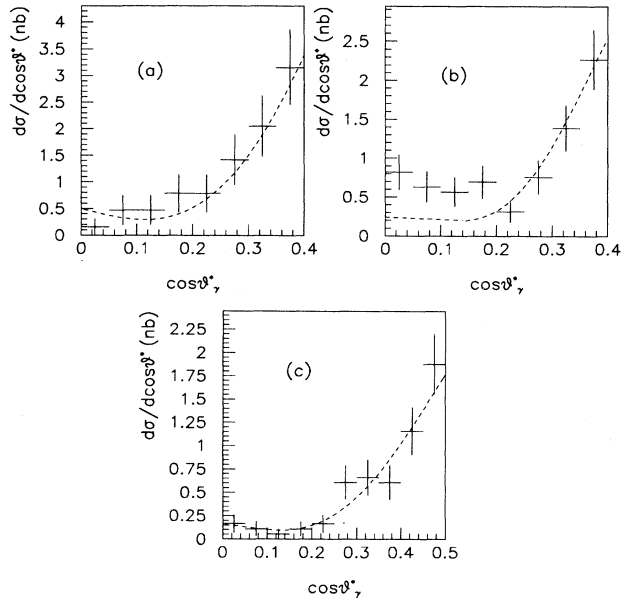

FIG. 10. Angular distribution of photons for data taken at 2.95 GeV (a), 2.99 GeV (b), and 3.097 GeV (c); the dashed curves are the result of a polynomial fit to the differential feed-down cross sections.

calculated *a priori*, by means of a simulation, that the value of the $|\cos\theta^*_\gamma|$ cut that maximizes the significance is ~ 0.25.

We fit the data with the maximum-likelihood method to the smooth background of Eq. (11) plus a Breit-Wigner line shape. For each energy point we had the measured center-of-mass energy (Table I, column 1), the normalized center-of-mass energy distribution $[f_j(\sqrt{s})]$, the integrated luminosity (Table I, column 2), and the number of $\bar{p}p \to \gamma\gamma$ candidates (Table I, column 3). The likelihood function was written, assuming Poisson statistics for the number (n_j) of events observed at the jth energy

$$L = \prod_{j=1,N} \frac{\nu_j^{n_j} e^{-\nu_j}}{n_j!} , \tag{15}$$

where[3]

$$\nu_j = \left[\int \mathcal{L}dt\right]_j \left[\sigma_{\rm back} + \int f_j(\sqrt{s})\sigma_m \times \frac{\Gamma^2_{\eta_c}}{4(\sqrt{s} - M_{\eta_c})^2 + \Gamma^2_{\eta_c}}\, d\sqrt{s}\right] \tag{16}$$

was the number of events expected at the jth energy point and

$$\sigma_m \equiv \frac{(2J+1)\pi}{k^2} B_{\bar{p}p} \times B_{\gamma\gamma} \times \text{efficiency} \times \text{acceptance} . \tag{17}$$

With a cut at $|\cos\theta^*_\gamma| = 0.25$, the efficiency $\times$ acceptance factor for our final data sample was $\epsilon_{\rm trigger} \times \epsilon_{\rm analysis} \times 0.25 = (0.91 \pm 0.02) \times (0.68 \pm 0.01) \times 0.25 = 0.155 \pm 0.004$.

$[\int \mathcal{L}dt]_j \sigma_{\rm back}$ [where $\sigma_{\rm back} = A \times (\sqrt{s_0}/\sqrt{s})^B \times$ efficiency $\times$ acceptance, and $\sqrt{s_0} = 2988.0$ MeV] was the expected number of background events within the angular range $|\cos\theta^*_\gamma| \le 0.25$, at the jth point.

The line in Fig. 6 shows the result of the fit to the data. From this fit we determined the two background parameters A and B and the resonance parameters: mass M_{η_c}, the width of the resonance Γ_{η_c}, and the product of branching ratios $B_{\bar{p}p} \times B_{\gamma\gamma}$ to the initial state and to the final state, which is proportional to the cross section at the peak of the resonance or, alternatively, $B_{\bar{p}p} \times B_{\gamma\gamma} \times \Gamma_{\eta_c} = B_{\bar{p}p} \times \Gamma_{\gamma\gamma}$, a quantity that measures the area under the resonance curve. The results of this fit are reported in the first column of Table IV.

The large errors in the resonance parameters can be substantially reduced if we assume that the background (which is poorly constrained by the four data points off resonance) is accurately described by the feed-down component. Further support for this hypothesis comes from a comparison of the measured cross section to the estimated feed-down cross section in the angular interval $0.25 < |\cos\theta^*_\gamma| \le 0.4$ (Fig. 11). In this angular interval the background component is dominant, and the resonance contributes at most 20% of the candidates, at peak energy. The open crosses in Fig. 11 represent the contribution that is expected from the η_c resonance in this acceptance interval calculated using the η_c parameters determined previously (Table IV, column 1). The solid circles show the measured cross sections with the resonance component subtracted. As can be seen, the feed-down calculation accurately describes the background even in the resonance region, leaving little room for the continuum process of Eq. (8).

We therefore performed a global maximum likelihood fit where the 11 data points of Table I are, as before, fit to the superposition of a resonance and a background described by Eq. (11), and the feed-down cross sections for $|\cos\theta^*_\gamma| \le 0.25$ (shown as open circles in Fig. 8) are fit to Eq. (11) only. In this way the parameters A and B of Eq. (11) are constrained both by the data and by the feed-down cross sections. In column 2 of Table IV we give the results of this fit. A comparison of the numbers reported in columns 1 and 2 shows that constraining the background with the feed-down data significantly reduces the statistical errors on the fitted parameters while keeping the central values almost unchanged. Column 2 represents our final result.

For our determination, taking $B_{\bar{p}p} = 12 \times 10^{-4}$ from Ref. [12], Γ_{η_c} is strongly correlated with both $B_{\gamma\gamma}$ ($\rho = -0.639$) and $\Gamma_{\gamma\gamma}$ ($\rho = 0.798$), as shown in the contour plots of Fig. 12. In contrast, the values of $B_{\gamma\gamma}$ and $\Gamma_{\gamma\gamma}$

[3]We used the general form although for wide resonances the unfolding of the center-of-mass energy distribution does not significantly affect the results.

TABLE IV. Comparison of different fits to η_c data.

$\cos\theta^*_\gamma$	0.0 - 0.25	0.0 - 0.25	0.0 - 0.15	0.0 - 0.2	0.0 - 0.3
M_{η_c} (MeV)	$2988.4^{+3.4}_{-3.3}$	$2988.3^{+3.3}_{-3.1}$	$2989.8^{+2.7}_{-2.5}$	$2988.8^{+2.4}_{-2.2}$	$2988.0^{+4.5}_{-5.8}$
Γ_{η_c}(MeV)	$25.9^{+18.6}_{-9.2}$	$23.9^{+12.6}_{-7.1}$	$17.2^{+8.2}_{-5.3}$	$19.0^{+8.0}_{-5.2}$	$31.4^{+28.7}_{11.7}$
$B_{\bar{p}p} \times B_{\gamma\gamma} \times 10^8$	$35.5^{+9.3}_{-9.4}$	$33.6^{+8.0}_{-7.0}$	$44.9^{+12.1}_{-10.3}$	$44.9^{+10.2}_{-8.8}$	$28.3^{+7.4}_{-6.4}$
$B_{\bar{p}p} \times \Gamma_{\gamma\gamma}$ (eV)	$9.2^{+7.1}_{-3.8}$	$8.1^{+2.9}_{-2.0}$	$7.7^{+2.6}_{-2.0}$	$8.6^{+2.5}_{-1.9}$	$8.9^{+5.8}_{-2.7}$
Events	222	222	124	175	314
λ	13.2	49.1	44.4	63.6	41.1
$\chi^2/N_{\rm DF}$	1.1	1.8	1.0	1.0	0.9
$N_{\rm DF}$	6	16	16	16	16
A (pb)	66.6 $\pm$15.4	71.4 $\pm$1.5	36.0 $\pm$1.1	49.0 $\pm$ 1.3	109.1 $\pm$1.9
B	26.0 $\pm$7.7	23.4$\pm$1.5	22.1 $\pm$2.1	23.1 $\pm$ 1.8	30.4 $\pm$1.5

are weakly correlated ($\rho = -0.201$). All contours are traced keeping the parameters M_{η_c}, A, and B fixed at their best fit values. Therefore contours that are traced for $\ln L_{\rm max} - 0.5$, $\ln L_{\rm max} - 2.0$, $\ln L_{\rm max} - 4.5$ do not correspond to 1, 2, 3 standard deviations. The values of the correlation coefficients (ρ) are the result of a complete regression analysis.

We studied the stability of the results against the $|\cos\theta^*_\gamma|$ cut by setting it at 0.15, 0.20, 0.25, and 0.30. The results are given in Table IV (columns 2–5). All errors shown in the table are statistical only. The value of A (the background cross section at the resonance peak energy) increases by a factor of 3 in the range of $|\cos\theta^*_\gamma|$ cuts examined. The values of the mass and of $B_{\bar{p}p} \times \Gamma_{\gamma\gamma}$, proportional to the area under the excitation curve, are stable. The two correlated parameters $B_{\bar{p}p} \times B_{\gamma\gamma}$, proportional to the height at peak energy, and Γ_{η_c}, the width of the excitation curve, are more sensitive to the fluctuations of the rapidly increasing background.

The parameter λ listed in Table IV measures the statistical significance of the signal. It is defined as $\lambda = 2 \times \ln(H1/H0)$ where $H1$ and $H0$ are the maximum values of the likelihood functions for the resonance

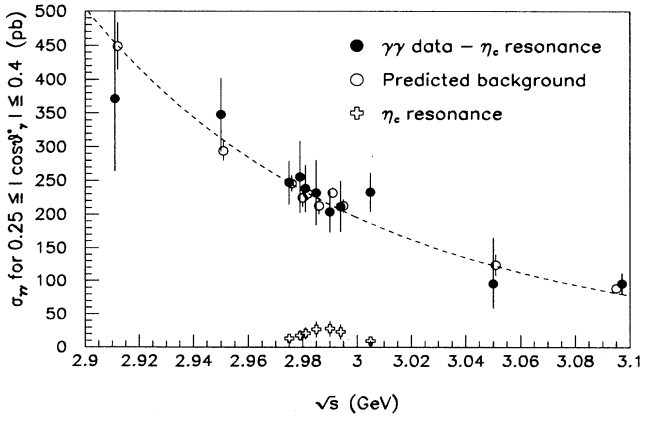

FIG. 11. Cross section for $\bar{p}p \to \gamma\gamma$ candidates in the angular interval $0.25 < |\cos\theta^*_\gamma| \leq 0.4$. The solid circles are the data from which the resonant component (open crosses) is subtracted. The line is the best fit of Eq. (11) to the predicted feed-down background (open circles).

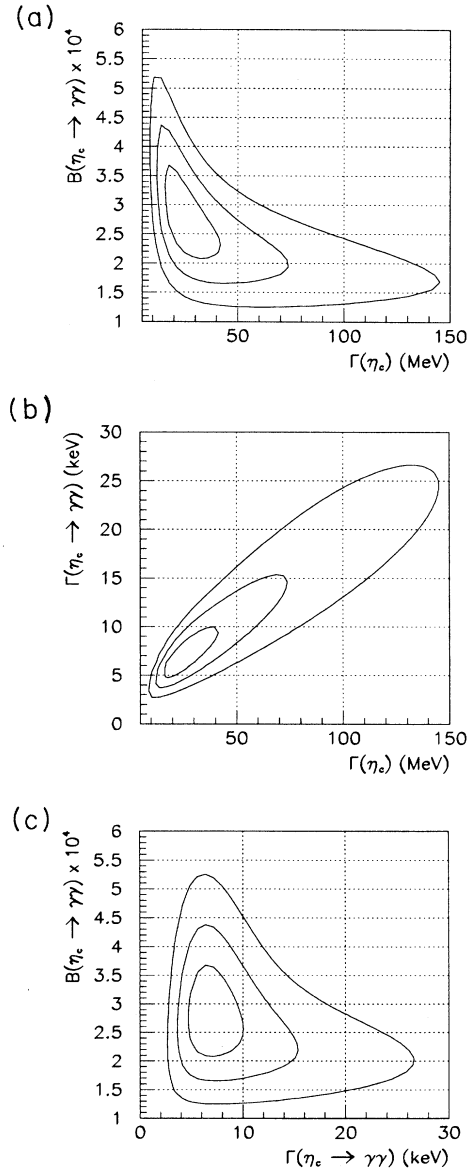

FIG. 12. (a) Likelihood contours of $B_{\gamma\gamma} \times 10^4$ vs Γ_{η_c} for the η_c resonance. (b) Likelihood contours of $\Gamma_{\gamma\gamma}$ vs Γ_{η_c} for the η_c resonance. (c) Likelihood contours of $B_{\gamma\gamma} \times 10^4$ vs $\Gamma_{\gamma\gamma}$ for the η_c resonance.

hypothesis ($H1$) and the null hypothesis ($H0$) (i.e., the hypothesis that the resonance is not present). In the limit of large statistics, $\sqrt{\lambda} \to n_\sigma$, the number of standard deviations above zero of the observed signal.

Finally, we present the values of the η_c parameters obtained from our experiment. We find, for the resonance mass,

$$M_{\eta_c} = 2988.3^{+3.3}_{-3.1}\ \text{MeV} . \tag{18}$$

The errors quoted are statistical. Additional uncertainties from the absolute energy calibration (0.1 MeV) and from the 0.5% point-to-point error in the luminosity measurement are negligible.

For the product of the branching ratio to $\bar{p}p$ times the partial width to two photons we find

$$B_{\bar{p}p} \times \Gamma_{\gamma\gamma} = (8.1^{+2.9}_{-2.0})\ \text{eV} . \tag{19}$$

The errors quoted are statistical. Compared to these, the contributions of errors in the measurement of the absolute luminosity and of the total efficiency ($\sim 4\%$ and $\sim 2\%$, respectively) are negligible. Using the Particle Data Group [12] value for $B_{\bar{p}p} = (12 \pm 4) \times 10^{-4}$ we obtain

$$\Gamma_{\gamma\gamma} = (6.7^{+2.4}_{-1.7} \pm 2.3)\ \text{keV} , \tag{20}$$

where the second error on $\Gamma_{\gamma\gamma}$ comes from the uncertainty in the $\bar{p}p$ branching ratio.

The fit result for the total width Γ_{η_c} is

$$\Gamma_{\eta_c} = 23.9^{+12.6}_{-7.1}\ \text{MeV} . \tag{21}$$

The errors quoted are statistical. Compared to these large statistical errors, contributions from the point-to-point uncertainty of the luminosity ($\sim 0.5\%$) are negligible.

We assumed in this analysis that the resonant amplitude does not interfere with the nonresonant process. We determined the nonresonant cross section to be about 20 pb (see Table III) to be compared with a peak resonant cross section of about 80 pb. We also observe that helicity conservation in perturbative QCD with massless constituents predicts that for $\bar{p} + p \to \gamma + \gamma$ the proton and antiproton have opposite helicities, which implies that a perturbative QCD (PQCD) allowed background does not interfere with η_c formation, where the proton and antiproton must have equal helicities.

A comparison of our results with previous measurements and with theoretical predictions appears in Fig. 13 and in Table V.

In the framework of PQCD one can in principle derive the value of the strong coupling constant α_s from the experimental value of $B_{\gamma\gamma} = \frac{\Gamma_{\gamma\gamma}}{\Gamma_{\text{tot}}} \approx \frac{\Gamma_{\gamma\gamma}}{\Gamma_{gg}}$, since ratios of rates for two annihilation processes of the same state only depend on the coupling constants. Unfortunately only calculations to next-to-leading order in α_s are available, leading to results that depend on the renormalization scheme and on the renormalization scale. Choosing the prescriptions of Ref. [13] we have

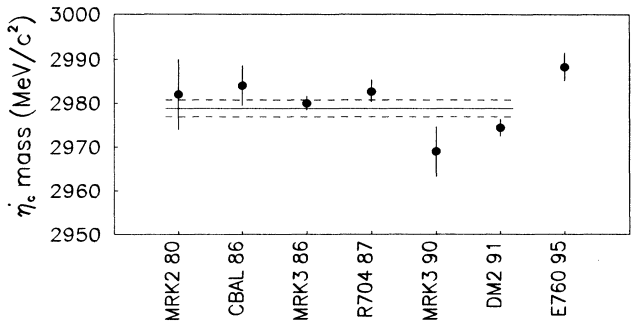

FIG. 13. Comparison of our result for the η_c mass value to values obtained by the Mark II [1], Crystal Ball [2], Mark III [3], R704 [11], and DM2 [3] Collaborations. The line represents the world average calculated from these measurements [12].

$$\frac{\Gamma_{\gamma\gamma}}{\Gamma_{gg}} \approx \frac{8}{9}\frac{\alpha^2}{\alpha_s^2}\left(\frac{1 - 3.4\alpha_s/\pi}{1 + 4.8\alpha_s/\pi}\right) . \tag{22}$$

From our measured branching ratio $B_{\gamma\gamma} = (2.80^{+0.67}_{-0.58} \pm 1.0) \times 10^{-4}$ we obtain the value

$$\alpha_s(m_c) = 0.29^{+0.05}_{-0.04} . \tag{23}$$

We point out that the value of $\frac{\Gamma_{\gamma\gamma}}{\Gamma_{gg}}$ is reduced by approximately a factor of 2 by the next-to-leading order correction. Additional factors to be taken into account include higher order terms, relativistic corrections, and the effect

TABLE V. Comparison with other measurements and theory.

	$B(\eta_c \to \gamma\gamma) \times B(\eta_c \to \bar{p}p)$ in units of 10^{-8}	$\Gamma(\eta_c \to \gamma\gamma)$ (keV)
Experiment		
E760	$33.6^{+8.0}_{-7.0}$	$6.7^{+2.4}_{-1.7} \pm 2.3$[a]
R704 [11]	68^{+42}_{-31}	$4.3^{+3.4}_{-3.7} \pm 2.4$
CLEO [7]		$5.73 \pm 1.34 \pm 1.98$
TPC [5]		$6.4^{+5.0}_{-3.4}$
PLUTO [4]		$33^{+15}_{-12} \pm 9$[b]
TASSO [6]		$19.9 \pm 6.1 \pm 8.6$
ARGUS [8]		11.3 ± 4.2
L3 [9]		$8.0 \pm 2.3 \pm 2.4$
Theory		
PQCD [13][c]		8.3 ± 0.8
B.A. [33]		3–5

[a]Using the Particle Data Group [12] value $B(\eta_c \to \bar{p}p) = (12 \pm 4) \times 10^{-4}$. The first error quoted come from our measurement while the second reflects the uncertainties in values taken from other experiments.

[b]Value calculated by us from the authors' measurement of $B(\eta_c \to K_S K^{\pm}\pi^{\mp}) \times B(\eta_c \to \gamma\gamma)$, using the Particle Data Group [12] value $B(\eta_c \to K\bar{K}\pi) = (6.6 \pm 1.8) \times 10^{-2}$. The first error quoted comes from their measurement while the second reflects the uncertainty in $B(\eta_c \to K\bar{K}\pi)$.

[c]$\Gamma(\eta_c \to \gamma\gamma) = \frac{4}{3}\left[1 + 1.96\frac{\alpha_s}{\pi}\right]\Gamma(J/\psi \to e^+e^-)$ with $\Gamma(J/\psi \to e^+e^-) = (5.26 \pm 0.37)$ keV [12] and $\alpha_s = 0.29^{+0.05}_{-0.04}$.

of a nonvanishing effective mass for the gluons [31], all of which may significantly alter the α_s dependence of Eq. (22) and affect the validity of our determination.

D. Results for the η_c' ($2\,^1S_0$)

In Fig. 14 the predictions for the angular distribution of the feed-down at $\sqrt{s} = 3619$ MeV are compared to the data taken at the same energy. The data closely follow the predictions, a feature common to all data taken at the six energy points, from $\sqrt{s} = 3590.8$ to $\sqrt{s} = 3621.1$ MeV (see Table II), where we searched for the η_c'. No evidence of a signal was seen at any of the six energy points. Since the angular distribution is flat for an S-wave resonance, while the predicted background shows a sharp rise above $|\cos\theta_\gamma^*| = 0.40$, only events with $|\cos\theta_\gamma^*| \leq 0.40$ were included in the sample. The number of events in this sample and the corresponding measured cross sections are presented in Table II and in Fig. 7, where the data at $\sqrt{s} = 3524$, 3626, 3668, and 3686 MeV are also given.

In the absence of a signal, we set upper limits on the product of the branching ratios $B(\eta_c' \to \bar{p}p) \times B(\eta_c' \to \gamma\gamma)$. These vary with $\sqrt{s}$ (because the data were not uniformly distributed in energy) and depend on the total width assumed for the η_c'. The upper limits (90% C.L.) on the product of branching ratios were calculated from the likelihood analysis described in Sec. IV C, using the ten data points reported in Table II. The free parameters in the fit were σ_m [Eq. (17)] and the two background parameters A and B [Eq. (11)]. The upper limit was defined by the value of σ_m for which $\ln L$ (where L is the likelihood function) was 0.819 of its maximum value. The product of branching ratios was obtained using Eq. (17). The efficiency × acceptance factor was, in this case, $\epsilon_{\text{trigger}} \times \epsilon_{\text{analysis}} \times 0.4 = (0.88 \pm 0.02) \times (0.61 \pm 0.03) \times 0.4 = 0.215 \pm 0.012$. The resulting 90% upper limits for the product of the branching ratios as a function of the η_c' mass are listed in Table VI for widths of 5 MeV, 10 MeV, and 15 MeV.

TABLE VI. Upper limits on the product $B(\eta_c' \to \bar{p}p) \times B(\eta_c' \to \gamma\gamma) \times 10^8$.

$\sqrt{s}$ (MeV)	$\Gamma_{\eta_c'} = 5$ MeV	$\Gamma_{\eta_c'} = 10$ MeV	$\Gamma_{\eta_c'} = 15$ MeV
3584.0	13.9	4.7	3.0
3586.0	7.8	3.2	2.3
3588.0	3.7	2.2	1.9
3590.0	2.0	1.7	1.6
3592.0	2.1	1.8	1.6
3594.0	3.4	2.1	1.8
3596.0	5.1	2.8	2.0
3598.0	9.5	3.6	2.3
3600.0	14.0	4.4	2.5
3602.0	14.9	4.4	2.4
3604.0	11.8	3.6	2.2
3606.0	7.6	2.7	1.7
3608.0	4.2	1.8	1.4
3610.0	2.0	1.2	1.2
3612.0	1.0	1.0	1.1
3614.0	1.1	1.1	1.2
3616.0	2.2	1.6	1.5
3618.0	4.8	2.9	2.2
3620.0	6.1	4.0	3.0
3622.0	7.4	5.1	3.8
3624.0	14.7	7.0	4.8

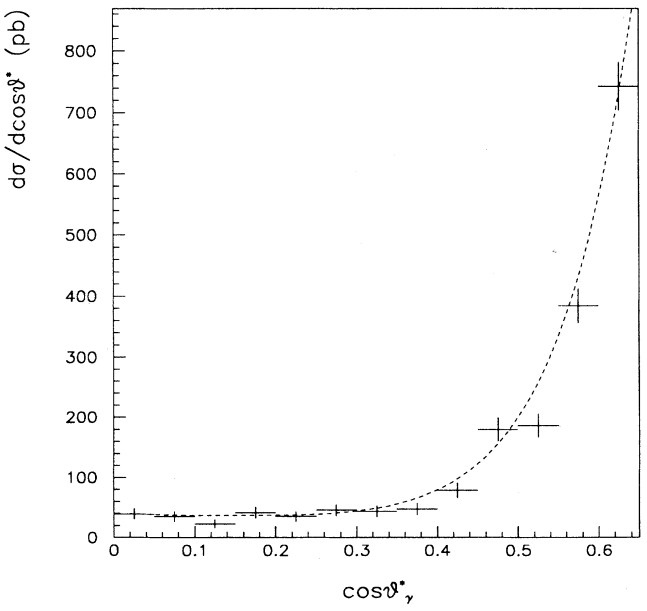

FIG. 14. Angular distribution of photons for data taken at 3.619 GeV; the dashed curve is the result of a polynomial fit to the differential feed-down background.

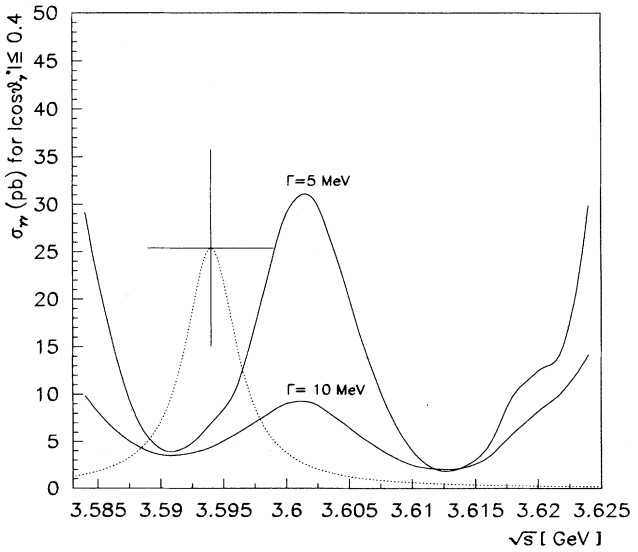

FIG. 15. 90% C.L. upper limits for $\sigma(\bar{p}p \to \eta_c' \to \gamma\gamma)$ at resonance peak in the acceptance interval $|\cos\theta_\gamma^*| \leq 0.4$ for a resonance of width Γ (solid lines). The dotted line shows our estimate of the signal expected for the Crystal Ball η_c' candidate with $\Gamma_{\eta_c'} = 5$ MeV. The horizontal error bar reflects the error in its mass while the vertical error bar shows the uncertainty in our estimate of $B(\eta_c' \to \bar{p}p) \times B(\eta_c' \to \gamma\gamma)$.

It is not straightforward to decide whether this result is in conflict with the observation, by the Crystal Ball Collaboration [10], of an η_c' candidate of mass 3594.0 ± 5.0 and width ≤ 8 MeV (95% C.L.). In our experiment the formation rate is proportional to $B(\eta_c' \to \bar{p}p)$ a quantity for which no firm prediction exists. We derived an estimate of $B(\eta_c' \to \bar{p}p)$ from $B(\eta_c \to \bar{p}p)$, assuming that the ratio $\frac{\Gamma(\bar{c}c \to \bar{p}p)}{\Gamma(\bar{c}c \to \text{gluons})}$, which for these states is well approximated by $B(\bar{c}c \to \bar{p}p)$, scales with energy in the same way as $\frac{\Gamma(\bar{c}c \to \bar{p}p)}{\Gamma(\bar{c}c \to \text{gluons})}$ for the J/ψ and for the ψ'. We observe, however, that since $\bar{p} + p \to \bar{c} + c$ for η_c and η_c' is suppressed (PQCD forbidden) [32], it is likely that the branching ratio for this process falls more rapidly with energy than the corresponding branching ratio for J/ψ and ψ' by an additional factor of s^{-1}. We take the value of $B(\eta_c' \to \gamma\gamma)$ to be equal to that we measured for $B(\eta_c \to \gamma\gamma)$. Our estimate of $B(\eta_c' \to \bar{p}p) \times B(\eta_c' \to \gamma\gamma)$ is $(12.3 \pm 5.0) \times 10^{-8}$ to be compared with our upper limit of 3.4×10^{-8} at $\sqrt{s} = 3594$ MeV, for $\Gamma_{\eta_c'} = 5$ MeV. (An illustration of this comparison is given in Fig. 15.)

V. SUMMARY AND CONCLUSIONS

The E760 Collaboration studied the reaction

$$\bar{p} + p \to \eta_c(1\,^1S_0) \to \gamma + \gamma \,. \tag{24}$$

We find the resonance mass to be $(9.5^{+3.8}_{-3.6})$ MeV higher than the current world average of (2978.8 ± 1.9) MeV [12].

From the same data we extracted the value of the product $B(\eta_c \to \bar{p}p) \times \Gamma(\eta_c \to \gamma\gamma)$. Dividing this quantity by $B(\eta_c \to \bar{p}p)$ [world average value $= (12 \pm 4) \times 10^{-4}$] we obtain $\Gamma(\eta_c \to \gamma\gamma) = (6.7^{+2.4}_{-1.7} \pm 2.3)$ keV, a value in agreement, within errors, with theoretical predictions and with the results of experiments that study the fusion of two virtual photons.

We quote a value for Γ_{η_c} which is significantly larger than the current world average. However, the measurement of this quantity is sensitive to background fluctuations, as suggested also by the observed drift of its central value with increasing angular acceptance.

We also performed a scan over a limited energy region searching for the η_c' resonance in the reaction

$$\bar{p} + p \to \eta_c'(2^1S_0) \to \gamma + \gamma \,. \tag{25}$$

The aim was to either confirm the result of the Crystal Ball experiment [10] or discover the η_c' at some other mass. As no signal was seen for the decay $\eta_c' \to \gamma\gamma$, we calculated upper limits for the product $B(\eta_c' \to \bar{p}p) \times B(\eta_c' \to \gamma\gamma)$, assuming that the η_c' has a total width $\Gamma_{\eta_c'}$ of 5, 10, or 15 MeV. We found that the 90% C.L. upper limits for the product of the branching ratios at $\sqrt{s} = 3594.0$ MeV were 3.4×10^{-8}, 2.1×10^{-8}, and 1.8×10^{-8} for $\Gamma_{\eta_c'}$ of 5, 10, and 15 MeV. These values can be compared to our phenomenologic estimate of $(12.3 \pm 5.0) \times 10^{-8}$ for the same quantity. Given the large uncertainty of this estimate we do not claim any compelling evidence against the Crystal Ball candidate.

We fit the data for the reaction

$$\bar{p} + p \to \gamma + \gamma \tag{26}$$

away from the η_c in order to estimate the continuum cross section. We observe no signal and set a 90% upper limit of 43 pb for $\sigma_{\bar{p}p \to \gamma\gamma}$ with $|\cos\theta_\gamma^*| \leq 0.4$ at $\sqrt{s} = 2988$ MeV.

ACKNOWLEDGMENTS

The authors wish to acknowledge the help of the members of the Fermilab Accelerator division. We also wish to thank the staff, engineers, and technicians at our respective institutions for their help and cooperation. We wish to thank in particular L. Bartoszek, C. Chizzo, E. Hahn, E. Harms, C. Kendziora, H. Koecher, D. McGinnis, J. Sasek, and J. Western (Fermilab); S. Bonora, V. Carassiti, G. Sorrentino, and L. Tracchi (Ferrara); G. Barisone, S. Minutoli, M. Negri, P. Poggi, and A. Pozzo (Genova); R. Tilden (Northwestern); J. Passaneau (Penn State); G. Algostino, F. Bertolino, F. Callá, D. Dattola, G. Dughera, R. Farano, and G. Giraudo (Turin). This research was supported by the U.S. Department of Energy, the U.S. National Science Foundation, and the Istituto Nazionale di Fisica Nucleare of Italy.

[1] T.M. Himel *et al.*, Phys. Rev. Lett. **45**, 1146 (1980).
[2] R. Partridge *et al.*, Phys. Rev. Lett. **45**, 1150 (1980); J.E. Gaiser *et al.*, Phys. Rev. D **34**, 711 (1986).
[3] R.M. Baltrusaitis *et al.*, Phys. Rev. Lett. **52**, 2126 (1984); Phys. Rev. D **33**, 629 (1986); Z. Bai *et al.*, Phys. Rev. Lett. **65**, 1309 (1990); D. Bisello *et al.*, Phys. Lett. B **179**, 289 (1986); Nucl. Phys. **B350**, 1 (1991).
[4] Ch. Berger *et al.*, Phys. Lett. **167B**, 120 (1986).
[5] H. Aihara *et al.*, Phys. Rev. Lett. **60**, 2355 (1988).
[6] C. Braunschweig *et al.*, Z. Phys. C **41**, 533 (1989).
[7] A. Bean *et al.*, in *Lepton and Photon Interactions*, Proceedings of the 16th International Symposium, Ithaca, New York, 1993, edited by P. Drell and D. Rubin, AIP Conf. Proc. No. 302 (AIP, New York, 1994), p. 779.
[8] H. Albrecht *et al.*, Phys. Lett. B **338**, 390 (1994).
[9] O. Adriani *et al.*, Phys. Lett. B **318**, 575 (1993).
[10] C. Edwards *et al.*, Phys. Rev. Lett. **48**, 70 (1982).
[11] C. Baglin *et al.*, Phys. Lett. **187B**, 191 (1987).
[12] Particle Data Group, L. Montanet *et al.*, Phys. Rev. D **50**, 1173 (1994).
[13] W. Kwong *et al.*, Phys. Rev. D **37**, 3210 (1988).
[14] T.A. Armstrong *et al.*, Phys. Rev. D **47**, 772 (1993); Nucl. Phys. **B373**, 35 (1992).
[15] M. Macri, in Proceedings of the 1983 CERN First Accelerator School: Antiprotons for Colliding Beam Facilities, Geneva, Switzerland, 1983, edited by P. Bryant and S. Newman [CERN Report No. 84-15, 1984, p. 469 (unpublished)].

[16] S.N. Gupta, W.W. Repko, and C.J. Suchyta III, Phys. Rev. D **39**, 974 (1989).
[17] *Total Cross Sections for Reactions of High Energy Particles*, edited by H. Schopper, Landolt-Börstein, New Series, Group X, Vols. I/12a and I/12b, Pt. X (Springer-Verlag, Berlin, 1988); T.A. Lasinski *et al.,* Nucl. Phys. **B37**, 1 (1972).
[18] S. Trokenheim *et al.,* Nucl. Instrum. Methods A **355**, 308 (1995).
[19] L. Bartoszek *et al.,* Nucl. Instrum. Methods A **301**, 47 (1991).
[20] R. Ray *et al.,* Nucl. Instrum. Methods A **307**, 254 (1991).
[21] I. Gaines *et al.,* Comput. Phys. Commun. **45**, 323 (1987); C. Gay *et al.*, IEEE Trans. Nucl. Sci. **NS-34**, 870 (1987).
[22] K.E. Gollwitzer, Ph.D. thesis, University of California, Irvine, 1993.
[23] J.E. Fast, Ph.D. thesis, University of California, Irvine, 1992.
[24] T.A. Armstrong *et al.,* Phys. Rev. Lett. **70**, 2988 (1993).
[25] G. Zioulas *et al.,* in Proceedings of the Third Biennial Conference on Low Energy Antiproton Physics, Bled, Slovenia, 1994 (unpublished); T.A. Armstrong *et al.,* "Two Body Final States Produced in Antiproton-Proton Annihilations at $2900 \leq \sqrt{(s)} \leq 3624$ MeV" (in preparation).
[26] G.R. Farrar *et al.,* Nucl. Phys. **B259**, 702 (1985); **B263**, 746(E) (1986); **B311**, 585 (1989).
[27] P. Kroll *et al.,* Phys. Lett. B **316**, 546 (1993).
[28] M. Artuso *et al.*, Phys. Rev. D **50**, 5484 (1994).
[29] T. Hyer, Phys. Rev. D **47**, 3875 (1993).
[30] T.A. Armstrong *et al.,* Phys. Rev. Lett. **70**, 1212 (1993).
[31] M. Consoli and J.H. Field, Phys. Rev. D **49**, 1293 (1994).
[32] S.J. Brodsky and G.P. Lepage, Phys. Rev. D **24**, 2848 (1981).
[33] E.S. Ackleh and T. Barnes, Phys. Rev. D **45**, 232 (1992); E.S. Ackleh, T. Barnes, and F.E. Close, *ibid.* **46**, 2257 (1992).

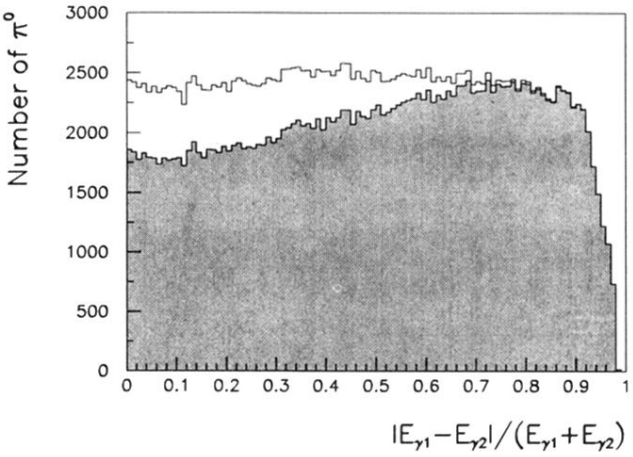

FIG. 4. Energy asymmetry in π^0 decays. The open histogram includes π^0's resolved by cluster splitting, while the shaded one does not.